Heterogeneous & Homogeneous & Bio-

CHEMCATCHEM

CATALYSIS

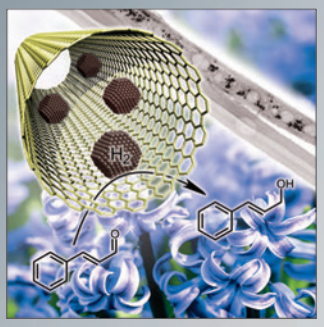

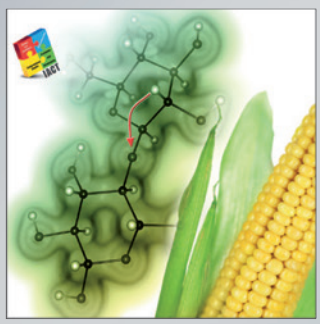

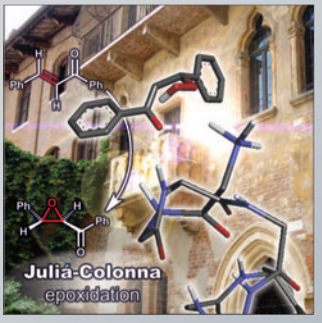

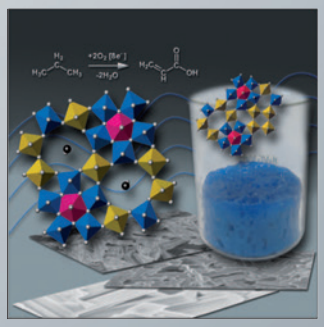

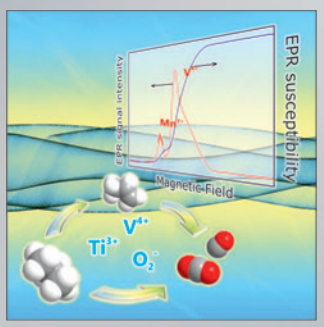

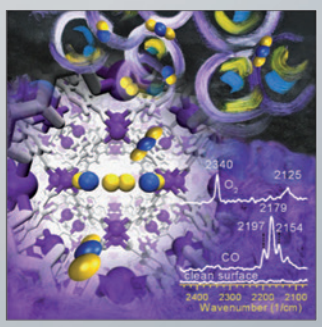

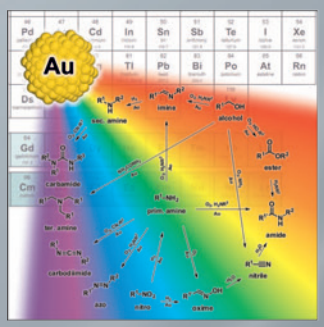

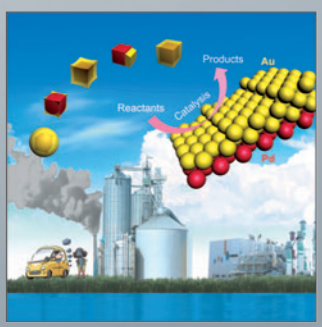

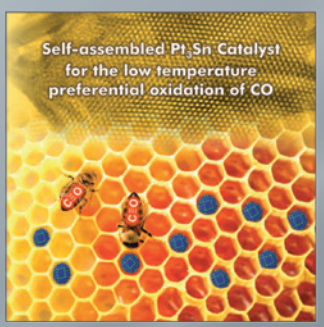

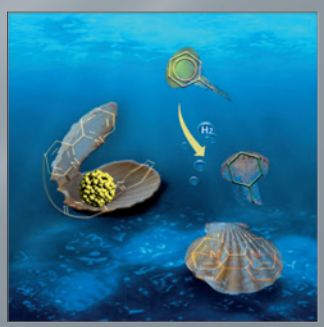

Reprint

© Wiley-VCH Verlag GmbH & Co. KGaA, Weinheim

A Journal of

ChemPubSoc Europe

WILEY-VCH

www.chemcatchem.org

ChemPubSoc Europe

DOI: 10.1002/cctc.201900175

CHEMCATCHEM Full Papers

Interplay Between Site Activity and Density of BCC Iron for Ammonia Synthesis Based on First-Principles Theory

Bing-Yan Zhang[+],[a, e] Hai-Yan Su[+],[b] Jin-Xun Liu,[c] and Wei-Xue Li*[d]

Site activity and density are two key factors in determining the overall activity of catalysts in heterogeneous catalysis. Combined DFT calculation, Wulff construction and micro-kinetic analysis, we reveal here a significant interplay between site activity and density of bcc iron catalyzed ammonia synthesis at low coverage regime. It is found that for large size particles, Fe (111) and (311) surfaces that consist of active C7 sites are limited by their low site density, whereas those with the most abundant sites are limited by their low activity. In contrast, Fe (221), (211) and (310) surfaces which consist of active C7 and/or B5 sites and remain abundant, dominate the overall reaction rate, turn-over-frequency and mass specific activity. Turn-over-frequency of the smaller Fe particles (2–6 nm) decreases by a factor of two or three due to the absence of (221) surface. For the particle size less than 2 nm, the corresponding activity decreases dramatically owing to the absence of all active C7 and/or B5 sites. Interplay of site abundance and intrinsic activity of catalysts is highlighted, and the insights revealed could be used to design and develop better catalysts for ammonia synthesis and other important reactions of technological interest.

Introduction

The synthesis of ammonia from nitrogen and hydrogen is an important process for the production of fertilizers, which has made huge contribution to world population growth during the past century.[1] The industrial importance has motivated a considerable scientific interest, and many fundamental concepts and techniques in heterogeneous catalysis are developed using the reaction as the prototype reaction.[2] The most common industrially used catalysts for this process are based on iron and ruthenium modified by the promoters, such as potassium etc.[3]

The ammonia synthesis is a structure-sensitive reaction, as first discovered by the variation of turnover number (TON) with iron particle size, the small iron particles (1.5 nm) having an order of magnitude lower TON than the large ones (4 nm) deposited on magnesia; with increasing iron particle size (30–150 nm), TON increases by 2–3 times compared with 4 nm iron particles.[4] The particle size effect has been attributed to the decrease in the concentration of the active C7 sites (iron atoms with seven nearest neighbors) on iron particles with decreasing particle size. The advances in surface science techniques and first-principles calculations establish a direct link between atomistic surface chemistry and catalytic activity, which greatly facilitates the understanding of the structure sensitivity.[5] Surface science studies using single crystals indicated that the open (111) and (211) crystal faces of iron, where the C7 sites exist, were the most active for N_2 dissociation-the generally believed rate determining step for ammonia synthesis.[2b,6] For ruthenium, the B5 sites (ensembles of five Ru atoms involving edge sites) have been shown to be the most active sites for N_2 dissociation.[2d] Theoretically, the intrinsic ammonia synthesis rate of various surface sites can be differentiated using a microkinetic simulation based on density functional theory (DFT) calculations of activation energies and stabilities of intermediates.[7] Norskov et al. took a further step to calculate the rate of ammonia synthesis over a nanoparticle ruthenium catalyst.[2d] They considered the stepped B5 sites as only active sites, and used the density of B5 sites to link with the size distribution of ruthenium particles supported on magnesium aluminum spinel measured by transmission electron microscopy, achieving the calculated rate within a factor of 3 to 20 of the measured rate.

Although the understanding toward structure effect in ammonia synthesis has progressed enormously, several fundamental questions still need to be settled. For instance, besides the well-studied (111) and (211) surfaces of body-centered

[a] B.-Y. Zhang[+]
State Key Laboratory of Catalysis
Dalian Institute of Chemical Physics
Chinese Academy of Sciences
Dalian 116023 (China)
[b] Prof. Dr. H.-Y. Su[+]
State Key Laboratory of Molecular Reaction Dynamics
Dalian Institute of Chemical Physics
Chinese Academy of Sciences
Dalian 116023 (China)
[c] J.-X. Liu
Department of Chemical Engineering
University of Michigan
Ann Arbor, MI 48109–2136 (USA)
[d] Prof. Dr. W.-X. Li
Department of Chemical Physics, Hefei National Laboratory for Physical Sciences at the Microscale
University of Science and Technology of China
Hefei 230026 (China)
E-mail: wxli70@ustc.edu.cn
[e] B.-Y. Zhang[+]
University of Chinese Academy of Sciences
Chinese Academy of Sciences
Beijing 100049 (China)
[+] These authors contributed equally to this work.

Supporting information for this article is available on the WWW under https://doi.org/10.1002/cctc.201900175

© 2019 Wiley-VCH Verlag GmbH & Co. KGaA, Weinheim

cubic(BCC) iron and step sites of face-centered cubic (FCC) ruthenium, many surface configurations such as specific open surfaces can also expose the C7 and B5 sites, respectively. Whether the C7 and/or B5 sites are more active for ammonia synthesis? Furthermore, the total activity of a catalytic reaction is not only related to the intrinsic activity of active sites, but their density on the metal nanoparticles.[2d,8] What are the ratios of the exposed surface sites on the metal nanoparticles and how do they depend on the particle size? Considering both intrinsic activity and density of active sites, which sites are the optimal sites amongst other sites exposed? Herein, we choose the BCC iron-based catalysts as probe materials, in an effort to address these important issues in ammonia synthesis. Combining the Wulff construction method with the density functional theory and microkinetic analysis, we investigate the intrinsic rate of ammonia synthesis on each surface sites exposed over BCC iron particles and the variation of the surface ratio of these surface sites with particle size from 0.7 nm to 15 nm. We clearly isolate the contribution of intrinsic rate of each surface sites and their density to the total reaction activity, and identify the optimal surface sites with varied particle size. With this understanding, we hope that the ammonia synthesis catalysts can be improved on the basis of fundamental insight.

Results and Discussion

Surface Energies and Wulff Construction

By a combination of surface energies (E_{surf}) calculations and Wulff construction, we first study the morphology of iron particle catalyst. The iron facets with miller indices $h+k+l\leq 5$ and $h\leq 3$ are investigated so that numerous iron facets with a large diversity in surface structure can be included. Apart from the well-studied (111) and (211) surface, (221),(311),(310) and (210), which can expose C7 and/or B5 sites are also considered in the present work. As shown in Table 1 and Figure 1, all the facets together with other low-energy facets expose on the Fe crystal morphology except (320) surface. The close-packed (110) surface has the lowest surface energy E_{surf} of 2.44 J/m^2, consisting of the largest ratio ($S=36\%$) of total surface area simultaneously. Besides (110) surface, the (310) and (211) surfaces, with the E_{surf} of 2.52 and 2.57 J/m^2, respectively, also cover a large ratio (28% and 25%) of total surface area. Despite the low E_{surf} (2.53 ~ 2.55 J/m^2), (100) and (210) expose relatively little owing to the symmetric influence. Specifically, the two surfaces are adjacent to (310) and (110) surface with very large

Table 1. Calculated surface energies (E_{surf}, J/m^2) and surface area proportion (S, %) of various BCC Fe facets.

(hkl)	E_{surf} [J/m^2]	S [%]	(hkl)	E_{surf} [J/m^2]	S [%]
(100)	2.53	4	(221)	2.63	3
(110)	2.44	36	(310)	2.52	28
(111)	2.69	0.4	(311)	2.60	2
(210)	2.55	1	(320)	2.54	/
(211)	2.57	25			

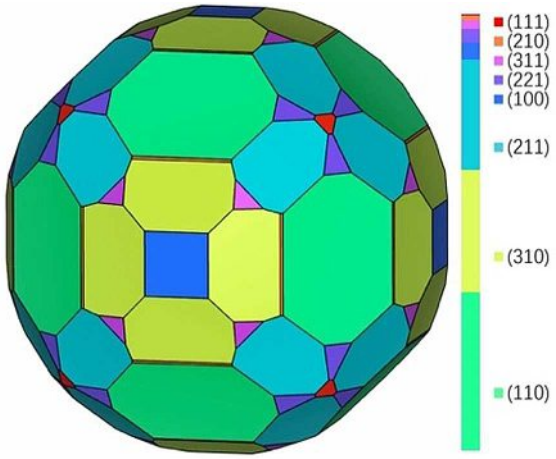

Figure 1. Equilibrium shape of BCC Fe crystal based on Wulff construction.

S, thereby leading to the reduction in surface area. The (111), (221) and (311) surfaces, where the C7 sites are available, only cover 5.4% surface area proportion in total due to their higher E_{surf}. Wulff construction suggests that the (211) surface has the largest S of all the surfaces that expose C7 sites over the iron catalyst.

Thermochemistry, Reaction Barrier and Geometry for Ammonia Synthesis

Having constructed the morphology of the iron particle catalyst, we then investigate the ammonia synthesis mechanism on all the eight iron surfaces exposed. The elementary steps, starting with N_2 dissociation and proceeding via sequential hydrogen addition to the resulting N atom, are considered here. The adsorption energies ΔE_{ads} of the intermediates involved on the iron surfaces are listed in Table 2. It is found that N_2 and H adsorption do not exhibit strong structure dependence, with the variation in ΔE_{ads} by 0.30 eV at most. Regardless of these iron surfaces, N_2 prefers a lying down structure at a 4 or 5-fold hollow site, as shown in Figure 2 (the C7 and/or B5 sites are highlighted). Compared to N_2 in gas phase, with the N–N bond length of 1.10 Å, the distance between two N atoms in

Table 2. Calculated adsorption energy ΔE_{ads} (eV) of various intermediates in ammonia synthesis.

(hkl)	E_{N2} [eV]	E_{N} [eV]	E_{NH} [eV]	E_{NH2} [eV]	E_{NH3} [eV]	E_{H} [eV]	E_{coNN} [eV]
(100)	−0.97	−1.66	−5.18	−3.22	−0.55	−0.40	−2.33
(110)	−0.89	−1.23	−5.34	−3.03	−0.48	−0.68	−0.75
(111)	−0.91	−1.15	−4.77	−3.24	−0.85	−0.53	−1.27
(210)	−0.92	−1.36	−5.20	−3.40	−0.72	−0.64	−1.71
(211)	−1.06	−1.03	−4.90	−3.54	−0.72	−0.53	−0.97
(221)	−0.80	−1.17	−5.28	−3.42	−1.02	−0.66	−1.02
(310)	−0.76	−1.42	−5.10	−3.43	−0.71	−0.63	−1.83
(311)	−1.04	−1.24	−5.03	−3.47	−0.86	−0.57	−1.51

© 2019 Wiley-VCH Verlag GmbH & Co. KGaA, Weinheim

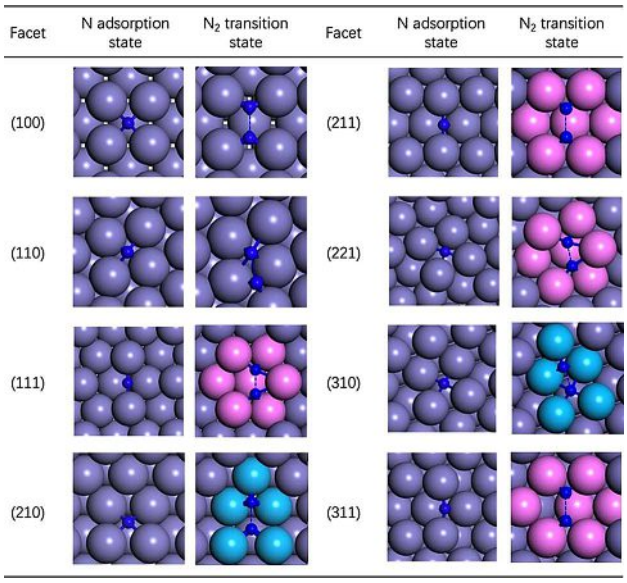

Figure 2. Structural information on N adsorption and transition state of N2 dissociation on BCC Fe facets. C7 and B5 sites are marked in pink and blue.

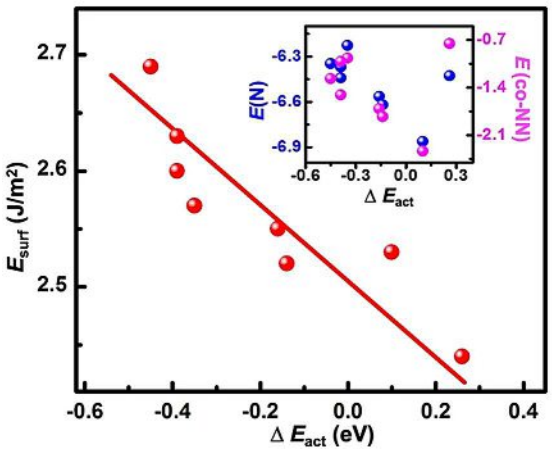

Figure 3. The calculated surface energies (E_{surf}) of BCC Fe surfaces as a function of activation energies (ΔE_{act}, relative to gaseous N_2) for N_2 dissociation (red). The insert figure shows the calculated N adsorption energies in separate (blue, E(N)) and co-adsorbed state (pink, E(co-NN)) as a function of ΔE_{act}.

adsorbed N_2 is elongated by 0.08–0.21 Å, suggesting that N–N bonds on the iron surfaces are activated.

NH_x (x = 0–3) adsorption, however, is more structure sensitive. On all the surfaces exposed, the variation of ΔE_{ads} falls in the range of 0.51 eV (N) −0.57 eV (NH). N and NH prefer 4-fold hollow site on all the surfaces (Figure 2), which can be divided into three types including square ((100), (210) and (310) facets), rhomboid ((110) and (221) facets) and saddle-like hollow sites ((111), (211) and (311) facets). The adsorption energy of N and NH on the three type sites generally follow the order of square > rhomboid > saddle-like hollow site, with the exception of (311) facet, which can be attributed to the surface reconstruction caused overestimation of ΔE_{ads}. As the number of H atom (x) increases, NH_x prefer less coordination with surface iron atoms. Specifically, NH_2 and NH_3 adsorb at the bridge and top sites on the iron surfaces, respectively.

Taking the most stable structure of N_2 adsorption as the initial state, we study N_2 dissociation on the eight iron surfaces exposed. The activation energies ΔE_{act}, reaction energy ΔH and the geometry at the transition state are listed in Table 3.

Table 3. The calculated activation energy for N_2 dissociation (ΔE_{act}, eV), reaction energy (ΔH, eV), the distance between two N atoms (d, Å), reaction rate over per active site (r, $s^{-1}site^{-1}$) in logarithm term and the yield contribution ratio (y_c, %) with respect to total yield.

(hkl)	ΔE_{act} [eV]	ΔH [eV]	d [Å]	log r	y_c [%]
(100)	0.10	−3.32	1.86	−4.06	0
(110)	0.26	−2.45	1.72	−2.15	0.3
(111)	−0.45	−2.29	1.68	0.86	1.6
(210)	−0.16	−2.73	1.79	−1.66	0
(211)	−0.35	−2.05	1.79	0.26	35.6
(221)	−0.39	−2.34	1.70	1.53	32.5
(310)	−0.14	−2.84	1.72	0.14	23.1
(311)	−0.39	−2.48	1.79	1.07	6.8

Interestingly, all the surfaces that expose C7 sites show rather high activity for N_2 dissociation; the ΔE_{act} of (111), (221), (311) and (211) slightly differ with each other from −0.35 to −0.45 eV, with the order of (111) > (221) = (311) > (211). Compared to the four surfaces, (210) and (310) are less active, and the ΔE_{act} are −0.16 eV and −0.14 eV, respectively. The (100) and (110) have the highest ΔE_{act} of 0.10 eV and 0.26 eV.

The correlation between the ΔE_{act} of N_2 dissociation and the ΔE_{ads} of N atoms in separate and co-adsorbed state on the iron surfaces is plotted in the insert of Figure 3. In general, the ΔE_{act} of N_2 dissociation decreases with decreasing ΔE_{ads} of N atoms (less negative) in separate and co-adsorbed state, in contradict with the traditional Bell-Evans-Polanyi (BEP) relation, which will lead to a ΔE_{ads}–ΔE_{act} relation with negative slope. This can be understood since the traditional BEP relation holds well for the surfaces with similar initial and transition state configuration. Because the same initial state of gaseous N_2 is used in this work, the different configurations at the transition states on the iron surfaces are responsible for the inapplicability of BEP relation. To include the effect from the different configurations, we use the surface energies E_{surf} of the iron surfaces to correlate with the ΔE_{act} of N_2 dissociation. Considering the large complexity of all the iron surfaces, a reasonable correlation between E_{surf} and ΔE_{act} of N_2 dissociation was demonstrated in Figure 3. The more stable the iron surfaces, the higher activation energies of N_2 dissociation.

Compared to N_2 dissociation, NH_x (x = 0–2) hydrogenation is less structure sensitive. As listed in Table 4, the variation of ΔE_{act} falls in the range of 0.25–0.50 eV on the iron surfaces when x increases from 0 to 2, less than that (0.71 eV) for N_2 dissociation. The thermochemistry and activation energy barriers of various elementary reactions of ammonia synthesis discussed above can be summarized in the energy profiles shown in Figure 4. Our results agree well with previous study on Ru surfaces in the sense that ammonia synthesis undergoes two strong exother-

© 2019 Wiley-VCH Verlag GmbH & Co. KGaA, Weinheim

Table 4. Calculated activation energy (ΔE_{act}, eV) and reaction energy (ΔH, eV) for three hydrogenation steps.

(hkl)	N + H→NH		NH + H→NH_2		NH_2 + H→NH_3	
	ΔE_{act} [eV]	ΔH [eV]	ΔE_{act} [eV]	ΔH [eV]	ΔE_{act} [eV]	ΔH [eV]
(100)	1.24	0.47	1.29	0.31	1.24	0.44
(110)	1.29	0.15	1.36	0.94	1.39	0.61
(111)	1.04	0.50	0.94	0.01	1.27	0.30
(210)	1.18	0.40	1.30	0.39	1.63	0.70
(211)	1.53	0.24	0.92	−0.16	1.34	0.72
(221)	1.34	0.14	1.42	0.47	1.30	0.45
(310)	1.24	0.54	1.13	0.26	1.49	0.73
(311)	1.27	0.37	1.25	0.08	1.38	0.57

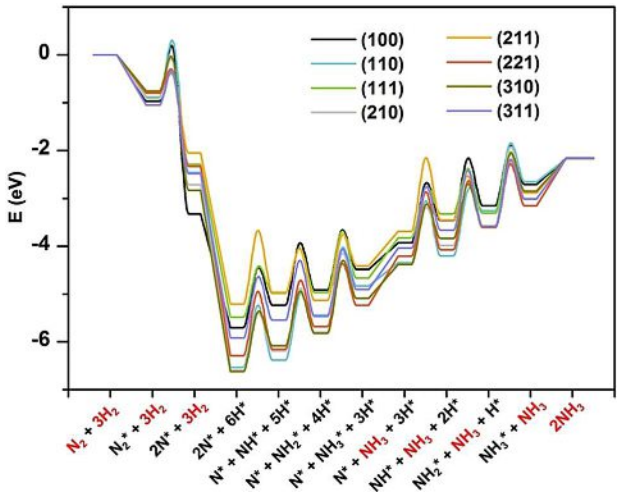

Figure 4. The energy profile for NH_3 synthesis over eight exposed BCC Fe surfaces. The molecules in red are in gas phase.

mic steps[2d] (N_2 and H_2 dissociation), followed by a serious of endothermic steps for NH_x hydrogenation (x = 0–2); N_2 dissociation have the highest transition state energies on the whole energy profiles.

Microkinetic Model

Based on the DFT calculated energy profiles above, a microkinetic simulation is conducted at typical ammonia synthesis condition (700 K, 100 bar, N_2:H_2:NH_3 = 1:3:0.01) using a full microkinetic model of MKMCXX package.[9] To better compare the relative difference of intrinsic reactivity of various iron facets, the reaction rate relative to (100) facet is shown in Figure 5 (see Table 3 for more details), which follows the order of (221) > (311) > (111) > (211) > (310) > (210) > (110), with 5.59, 5.13, 4.92, 4.32, 4.19, 2.40 and 1.90 orders of magnitude higher than (100) facet, respectively. The calculated reactivity trend is in good agreement with the experimental results[2b] that (111) and (211) have reaction rate higher than (210) and (110) facets. Besides the C7 sites on (111) and (211) reported by previous experimental studies, we find another two active C7 sites on

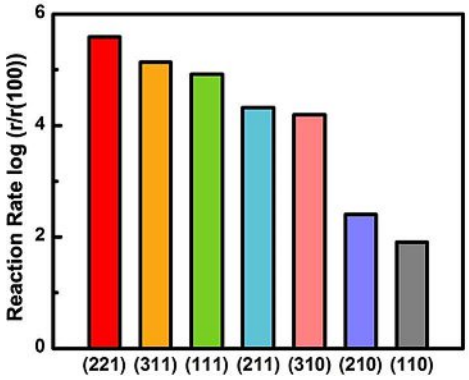

Figure 5. The calculated reaction rate over per active site based on Wulff construction morphology.

(221) and (311), together with one active B5 site on (310), and all the sites are very active for ammonia synthesis.

Apart from the intrinsic activity, the number of active sites available also has a significant influence on the total reaction activity. We thus define the facet yield contribution ratio $r_{c,i}$ [Eq. (1)]:

$$r_{c,i} = (r_i \times S_i/A_i)/\Sigma(r_i \times S_i/A_i) \quad (1)$$

where r_i, S_i, A_i are reaction rate, surface area proportion and (1 × 1) active site area of facet i, respectively. The larger $r_{c,i}$ value a surface possesses, the larger it contributes to the total reactivity. As listed in Table 3, (211), (221) and (310) facet shows the largest $r_{c,i}$ based on the consideration of both intrinsic activity and the number of active sites, dominating 91.2% of the total yield. The remaining facets are limited by either low intrinsic activity, such as (110), (100) and (210), or by the low density of active sites, such as (111) and (311). Interestingly, of all the surfaces that expose C7 sites and/or B5 sites, the least active (211) and (310) act as the optimal active sites. These results indicate that the density of active sites can play a key role when the surfaces have close intrinsic activity. In our previous work,[8] the important role of density of active sites in Ru catalyzed Fischer-Tropsch synthesis has been identified. Although the lowest CO dissociation barrier of FCC Ru remains higher than that of HCP Ru, is site abundance by more than two orders of magnitude leads to the corresponding mass specific activity three times higher. Inorganic synthesis of specific morphology that expose more active sites, identified as desired catalysts by first principles, is expected to improve catalytic activity for ammonia synthesis.

Particle Size Effect of Iron Based Ammonia Synthesis

It has been identified that the large iron particles, with the particle size of 30–150 nm, have 2–3 times and an order of magnitude higher TON than the small iron particles (4 nm and 1.5 nm) in ammonia synthesis.[4a,b] The particle size effect has been ascribed to the decrease in the ratio of the active sites on

© 2019 Wiley-VCH Verlag GmbH & Co. KGaA, Weinheim

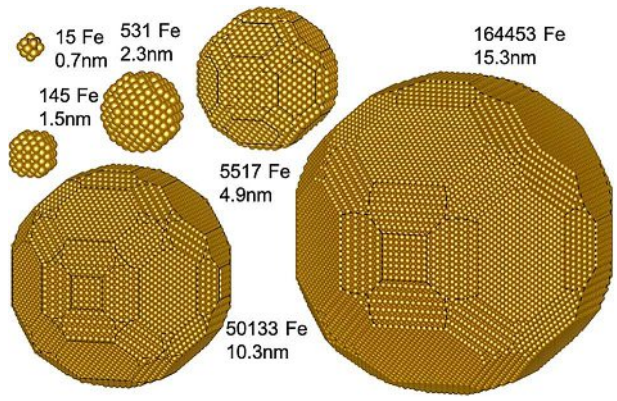

Figure 6. BCC Fe particle structures with particle size varying from 0.7 nm to 15 nm.

iron particles with decreasing the particle size. However, it remains unclear how the structures of iron catalysts, particularly those of iron surfaces exposing C7 and/or B5 sites, depend on particle size, which calls for a fundamental understanding at the atomic level.

To provide insights into this question, BCC iron particles with increasing size from 0.7 nm to 15 nm were built based on Wulff construction, as shown in Figure 6. At a small particle size of 1.5 nm, only the close-packed (110) and (100) surface with 145 iron atoms in total are exposed. As the particle size increases, more and more active surfaces appear in the morphology of iron catalyst. For instance, (211), (310), (221) and (111) & (311) become available when the particle size is larger than 2 nm, 5 nm, 10 nm and 15 nm, respectively. The (210) surface that can be exposed on the larger iron particle surface as discussed above, is not be observed in the particle size range (0.7–15 nm) studied. The size dependent morphology can be due to the effect of both surface area ratio and crystallographic symmetry. Having identified the morphology of iron catalyst at different particle size, we then investigate the activity of ammonia synthesis on the iron particles. Based on the reaction rate on each facet exposed, we calculated the overall reaction rate *r*, turnover frequency (TOF) and mass specific activity (MSA) as a function of particle size in Figure 7. The activity of Fe particles can be given by [Eq. (2)–(4)]:

$$r = \sum_i n_i \times r_i \tag{2}$$

$$TOF = \sum_i n_i \times r_i / \sum_i n_i \tag{3}$$

$$\mathrm{MSA} = \sum_i n_i \times r_i / (N \times m_{\mathrm{atom}}) \tag{4}$$

where n_i and r_i are the number of active sites and reaction rate (Eq.3) for facet i, N is the total number of atom in a given particle. Note that no migration or diffusion of surface species between the facets is considered in the assessment of Fe particle activity.

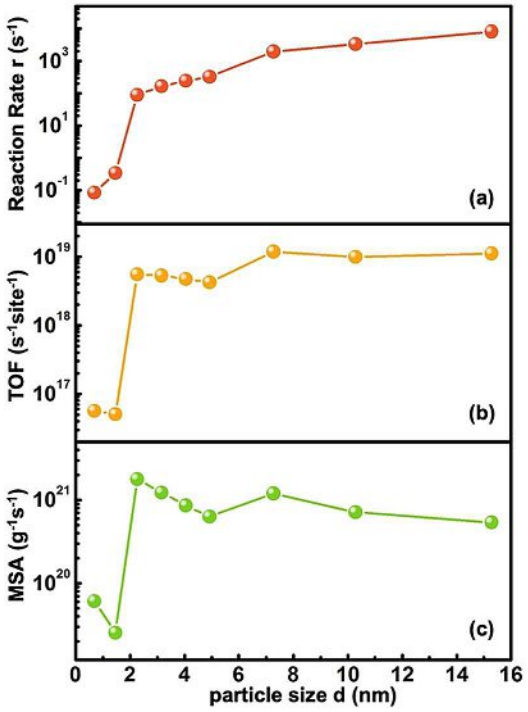

Figure 7. The calculated (a) the overall reaction rate (r, s^{-1}), (b) turnover frequency (TOF, $site^{-1}s^{-1}$) and (c) mass specific activity (MSA, $g^{-1}s^{-1}$) as a function of particle size on BCC Fe particles.

It can be seen that the total reaction rate, TOF and MSA exhibit similar trend with the particle size, which can be divided into three stages. The activity of ammonia synthesis decreases sharply for iron particle size below 2.3 nm. At larger particle sizes (2.3–6 nm), the overall reaction rate, TOF and MSA increases dramatically and varies with different trend with size. As the particle size increases further, the total reaction rate (Figure 7a) increases slightly; the TOF (Figure 7b) keeps almost constant, and the MSA (Figure 7c) decreases slightly. The similar reaction activity trend also holds in the larger particles (6–15 nm), but with a higher reaction activity.

Figure 8 shows the yield of each facet relative to total yield as a function of iron particle size. It is found that the high yield of (211), (310) and (221) facet predominate the total yield when the particle size is larger than 6 nm, and thereby resulting in the unchanged TOF. The slight increase in the overall reaction rate with particle size mainly originates from increased number of active sites. However, the decrease in the specific surface area is responsible for the decrease in MSA with particle size. For the smaller particles with size from 2.3 nm to 6 nm, (221) facet cannot be exposed anymore due to its large unit cell of 24 $Å^2$, compared to 12.7 $Å^2$ and 9.8 $Å^2$ for (310) and (211), respectively. As a result, corresponding TOF is lower. For particle size smaller than 2 nm, (310) and (211) facet also disappear, and instead (100) and (110) facets are exposed. Their substainally lower intrinsic activities decrease dramatically the overall reactivity at this range of size. The calculated TOF values (Figure 7b) are in excellent agreement with previous exper-

© 2019 Wiley-VCH Verlag GmbH & Co. KGaA, Weinheim

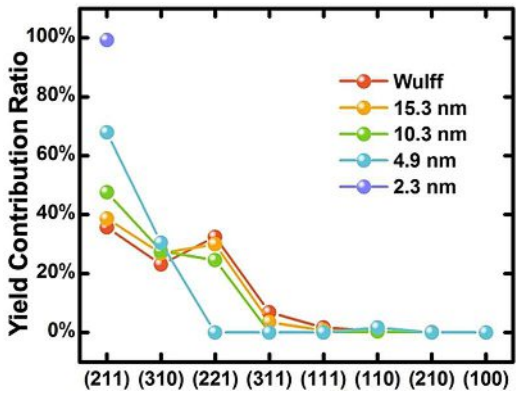

Figure 8. The yield contribution ratio of 8 exposed surfaces at various size of BCC Fe particles for ammonia synthesis.

imental findings, in which the large iron particles (>6 nm) have 2–3 times higher TOF than the small iron particles of 2–6 nm, and an order of magnitude of higher TOF than that less than 2 nm.

So far, the discussions of structure sensitivity for iron-based ammonia synthesis primarily focus on the intrinsic activity. The iron (111) and (211) surfaces, where the C7 sites are available, have been shown to be more active than the close packed surfaces for ammonia synthesis. In the present work, we identify another two C7 sites on (311) and (221) and one B5 site on (310), which are also very active. In this case, the density of active site is crucial in determining which surface sites dominate the overall reaction activity. The combination of DFT calculation, Wulff construction and micro-kinetic analysis enables to differentiate the contribution of intrinsic activity and density of active sites to the total reaction activity. We show here that the (211), (310) and (221) surface dominate the total reaction activity for iron particles larger than 6 nm, which also lead to the constant TOF at this size range. However, with the missing of all C7 and/or B5 sites at smaller particle size (<2 nm), the TOF values are substantially reduced compared to those at larger particle size. The isolation of the contribution of intrinsic activity and density of active sites by theoretical method can guide material synthesis with desirable morphology. With the development of material synthesis methods, we hope that the ammonia synthesis catalysts can be improved based on the fundamental understanding.

We note Wulff construction which can be used to study the particle morphology under thermodynamic equilibrium conditions, will do not apply for those under out-of-equilibrium conditions. The energy contribution due to edge and corner atoms is ignored in Wulff construction, which may lead to the deviation of particle morphology from real case, particularly for the smaller particles. Several recent works employed a modified broken bond model and the embedded atom model to simulate explicitly the morphology of Co nanoparticles,[10] which should be applied similarly for iron nanoparticles in future. Moreover, the present work only focuses on the low coverage regions, and the coverage and lateral interaction could have pronounced influence on the structural sensitivity and size effect. Nevertheless, once the energy profile on individual facet exposed and corresponding intrinsic activity derived for instance by microkinetics program at higher coverage are available, the framework developed in the present work together with site percentage could be applied, and the resulted activity could be compared directly to the experiments.

Conclusions

Combined DFT calculation, Wulff construction and micro-kinetic analysis, we present a theoretical study of ammonia synthesis on the BCC iron catalysts at the low coverage regime. The effect of intrinsic activity and the density of active sites on overall reaction activity are differentiated, and their dependence on particle size is also addressed. It is found that Fe (111) and (311) surfaces that consist of highly active C7 sites are limited by the low surface area proportion exposed, whereas those with highest surface area proportion exposed, such as Fe (110) and (310) are limited by their low intrinsic activity. Fe (211), (310) and (221) surface, which consist of active C7 and/or B5 sites and remain abundant, dominate the overall reactivity when iron particles are larger than 6 nm, leading to the stable turn-over-frequency. With further decreasing the particle size down to 2.3–6 nm, corresponding turn-over-frequency is lowered by a factor of two or three, due to the absence of the highly active Fe (221) surface. At smaller particle size (less than 2 nm), however, the reactivity is substantially reduced because no active C7 and/or B5 sites are exposed, instead only the facets with the lower intrinsic activity are exposed. This work highlights the impact of density of active sites and particle morphology in catalytic reactions, and the fundamental understanding achieved can potentially be used to design and develop improved catalysts for ammonia synthesis and other important reactions of technological interest.

Computational methods and models

All the spin-polarized density functional theory (DFT) calculations were carried out using Projector augmented wave (PAW) potentials[11] and generalized gradient approximation (GGA) with Perdew-Burke-Ernzerhof (PBE) exchange-correlation functions,[12] implemented in Vienna ab initio simulation package (VASP).[13] The kinetic-energy cutoff of 400 eV was used to expand the electronic wave functions. Calculation of bulk BCC Fe (α-Fe) with a k-point mesh[14] of 10×10×10 gives an equilibrium lattice constant of 2.832 Å and a local spin magnetic moment of 2.185 μ_B, which are in good agreement with previous calculation[15] and experiment.[16] For surface energy calculations of BCC Fe (100), (110), (111), (210), (211), (221), (310), (311) and (320), the p(1×1) slab models with clean facet thickness of ~20 Å separated by a vacuum layer of 15 Å were used. The density of k-points was set at ~0.03 $Å^{-1}$, as 12×12×1 k-point sampling for (100) surface. The equilibrium shape of BCC Fe crystal and various sized particles of BCC Fe can be constructed with these calculated surface energies in VESTA software package[17] using Wulff construction method.[18] In our calculations, surface energy is determined from the relation $E_{surf}=(E_{slab}-N\times E_{bulk})/2\,A$, where E_{slab} is the total energy of the slab and $N\times E_{bulk}$ is the total

© 2019 Wiley-VCH Verlag GmbH & Co. KGaA, Weinheim

energy of the number of N bulk Fe atoms in the slab. A is surface area and the factor 2 accounts for the presence of two surfaces. All adsorptions of reaction intermediates (N2*, N*, H*, NH*, NH2* and NH3*) and transition states (N–N, N–H, HN–H and H2N–H) involved in synthesis ammonia were calculated with the p(2×2) slab models. A p(3x3) slab is used to calculate NH2* hydrogenation to NH3* on close-packed Fe (110), and an activation energy differing of 0.08 eV only from p(2x2) slab is found, which suggests that the p(2×2) slab is sufficient for the present study. The facet thickness was set to ~10 Å separated by a vacuum layer of 15 Å with ~0.04 $Å^{-1}$ k-point density. The transition states of N2 decomposition and hydrogenation steps were verified by improved force reversed method.[19] The reaction rate was calculated by a full microkinetic model of MKMCXX package.[9]

Acknowledgements

We acknowledge funding from the National Key R&D Program of China (2018YFA0208603, 2017YFB0602205, 2017YFA0204800), the Chinese Academy of Sciences (QYZDJ-SSW-SLH054), and Natural Science Foundation of China (91645202, 21872136).

Conflict of Interest

The authors declare no conflict of interest.

Keywords: Heterogeneous Catalysis · Density Functional Calculations · Iron · Kinetics · Ammonia synthesis

[1] a) A. Mittasch, *Adv. Catal.* **1950**, *2*, 81–104; b) J. W. Erisman, M. A. Sutton, J. Galloway, Z. Klimont, W. Winiwarter, *Nat. Geosci.* **2008**, *1*, 636–639; c) H. Z. Liu, *Chin. J. Catal.* **2014**, *35*, 1619–1640.

[2] a) N. D. Spencer, R. C. Schoonmaker, G. A. Somorjai, *J. Catal.* **1982**, *74*, 129–135; b) D. R. Strongin, J. Carrazza, S. R. Bare, G. A. Somorjai, *J. Catal.* **1987**, *103*, 213–215; c) R. Schlogl, *Angew. Chem. Int. Ed.* **2003**, *42*, 2004–2008; d) K. Honkala, A. Hellman, I. N. Remediakis, A. Logadottir, A. Carlsson, S. Dahl, C. H. Christensen, J. K. Norskov, *Science* **2005**, *307*, 555–558; e) J. H. Montoya, C. Tsai, A. Vojvodic, J. K. Norskov, *ChemSusChem* **2015**, *8*, 2180–2186.

[3] a) K. Aika, A. Ozaki, H. Hori, *J. Catal.* **1972**, *27*, 424–431; b) S. R. Bare, D. R. Strongin, G. A. Somorjai, *J. Phys. Chem.* **1986**, *90*, 4726–4729; c) D. R. Strongin, G. A. Somorjai, *J. Catal.* **1989**, *118*, 99–110; d) C. J. H. Jacobsen, S. Dahl, P. L. Hansen, E. Tornqvist, L. Jensen, H. Topsoe, D. V. Prip, P. B. Moenshaug, I. Chorkendorff, *J. Mol. Catal. A* **2000**, *163*, 19–26; e) H. Bielawa, O. Hinrichsen, A. Birkner, M. Muhler, *Angew. Chem. Int. Ed.* **2001**, *40*, 1061–++; f) C. F. Huo, B. S. Wu, P. Gao, Y. Yang, Y. W. Li, H. J. Jiao, *Angew. Chem. Int. Ed.* **2011**, *50*, 7403–7406; g) M. Hara, M. Kitano, H. Hosono, *ACS Catal.* **2017**, *7*, 2313–2324.

[4] a) J. A. Dumesic, H. Topsoe, S. Khammouma, M. Boudart, *J. Catal.* **1975**, *37*, 503–512; b) J. A. Dumesic, H. Topsoe, M. Boudart, *J. Catal.* **1975**, *37*, 513–522; c) G. Ertl, S. B. Lee, M. Weiss, *Surf. Sci.* **1982**, *114*, 527–545; d) J. J. Mortensen, L. B. Hansen, B. Hammer, J. K. Norskov, *J. Catal.* **1999**, *182*, 479–488; e) S. Dahl, A. Logadottir, R. C. Egeberg, J. H. Larsen, I. Chorkendorff, E. Tornqvist, J. K. Norskov, *Phys. Rev. Lett.* **1999**, *83*, 1814–1817; f) R. C. Egeberg, S. Dahl, A. Logadottir, J. H. Larsen, J. K. Norskov, I. Chorkendorff, *Surf. Sci.* **2001**, *491*, 183–194; g) S. J. Jenkins, *Surf. Sci.* **2006**, *600*, 1431–1438.

[5] a) R. A. Van Santen, *Acc. Chem. Res.* **2009**, *42*, 57–66; b) J. Greeley, M. Mavrikakis, *Nat. Mater.* **2004**, *3*, 810–815; c) L. Li, A. H. Larsen, N. A. Romero, V. A. Morozov, C. Glinsvad, F. Abild-Pedersen, J. Greeley, K. W. Jacobsen, J. K. Norskov, *J. Phys. Chem. Lett.* **2013**, *4*, 222–226.

[6] G. A. Somorjai, N. Materer, *Top. Catal.* **1994**, *1*, 215–231.

[7] a) A. Logadottir, T. H. Rod, J. K. Norskov, B. Hammer, S. Dahl, C. J. H. Jacobsen, *J. Catal.* **2001**, *197*, 229–231; b) T. Bligaard, J. K. Norskov, S. Dahl, J. Matthiesen, C. H. Christensen, J. Sehested, *J. Catal.* **2004**, *224*, 206–217; c) I. Chorkendorff, J. W. Niemantsverdriet, *Concepts of modern catalysis and kinetics*, 2nd, rev. and enlarged ed., Wiley-VCH, Weinheim, **2007**; d) S. Dahl, J. Sehested, C. J. H. Jacobsen, E. Tornqvist, I. Chorkendorff, *J. Catal.* **2000**, *192*, 391–399; e) G. Ertl, *Adv. Catal.* **2000**, *45*, 1–69; f) J. Cheng, P. Hu, P. Ellis, S. French, G. Kelly, C. M. Lok, *J. Phys. Chem. C* **2008**, *112*, 1308–1311; g) J. Qian, Q. An, A. Fortunelli, R. J. Nielsen, W. A. Goddard, *J. Am. Chem. Soc.* **2018**, *140*, 6288–6297.

[8] W. Z. Li, J. X. Liu, J. Gu, W. Zhou, S. Y. Yao, R. Si, Y. Guo, H. Y. Su, C. H. Yan, W. X. Li, Y. W. Zhang, D. Ma, *J. Am. Chem. Soc.* **2017**, *139*, 2267–2276.

[9] I. A. W. Filot, R. A. van Santen, E. J. M. Hensen, *Angew. Chem. Int. Ed.* **2014**, *53*, 12746–12750.

[10] a) P. van Helden, I. M. Ciobica, R. L. J. Coetzer, *Catal. Today* **2016**, *261*, 48–59; b) R. Agrawal, P. Phatak, L. Spanu, *Catal. Today* **2018**, *312*, 174–180.

[11] P. E. Blochl, *Phys. Rev. B* **1994**, *50*, 17953–17979.

[12] J. P. Perdew, K. Burke, M. Ernzerhof, *Phys. Rev. Lett.* **1996**, *77*, 3865–3868.

[13] a) G. Kresse, J. Hafner, *Phys. Rev. B* **1993**, *47*, 558–561; b) G. Kresse, J. Furthmuller, *Phys. Rev. B* **1996**, *54*, 11169–11186.

[14] H. J. Monkhorst, J. D. Pack, *Phys. Rev. B* **1976**, *13*, 5188–5192.

[15] D. C. Sorescu, *Phys. Rev. B* **2006**, *73*.

[16] C. Kittel, *Introduction to Solid State Physics*, Wiley, New York, **1996**.

[17] K. Momma, F. Izumi, *J. Appl. Crystallogr.* **2011**, *44*, 1272–1276.

[18] G. Wulff, *Z. Kristallogr. Mineral.* **1901**, *34*, 449–530.

[19] K. J. Sun, Y. H. Zhao, H. Y. Su, W. X. Li, *Theor. Chem. Acc.* **2012**, *131*.

Manuscript received: January 29, 2019
Accepted manuscript online: February 20, 2019
Version of record online: March 7, 2019

© 2019 Wiley-VCH Verlag GmbH & Co. KGaA, Weinheim